KeAi

CHINESE ROOTS
GLOBAL IMPACT

#### Contents lists available at ScienceDirect

## Petroleum Science

journal homepage: www.keaipublishing.com/en/journals/petroleum-science



## Original Paper

## Experimental study of a circulation agent dynamic plugging for multi-scale natural fractures



Zhao-Wen Hu a,b, Yi-Qun Zhang a,b,\*, Jin-Shan Wang b, Xin-Yu Wang b, Yu Qin b, Ya Liu c

- <sup>a</sup> State Key Laboratory of Deep Geothermal Resources, China University of Petroleum-Beijing, Beijing, 102249, China
- b College of Safety and Ocean Engineering, China University of Petroleum-Beijing, Beijing, 102249, China
- <sup>c</sup> Sinopec Oilfield Service Corporation, Beijing, 100101, China

#### ARTICLE INFO

Article history:
Received 18 December 2024
Received in revised form
15 July 2025
Accepted 18 July 2025
Available online 28 July 2025

Edited by Jia-Jia Fei

Keywords: Dynamic plugging Large scale fracture Lost circulation material Laboratory experiments Fracture aperture

#### ABSTRACT

Lost circulation critically jeopardizes drilling safety and efficiency, and remains an unresolved challenge in oil and gas engineering. In this paper, by utilizing the self-developed dynamic plugging apparatus and synthetic cores containing large-scale fractures, experimental research on the circulation plugging of different materials was conducted. Based on the D90 rule and fracture mechanical aperture model, we analyze the location of plugging layer under dynamic plugging mechanism. By setting different parameters of fracture width and injection pressure, the laws of cyclic plugging time, pressure bearing capacity and plugging layers formation were investigated. The results show that the comprehensive analysis of particle size and fracture aperture provides an accurate judgment of the entrance-plugging phenomenon. The bridging of solid materials in the leakage channel is a gradual process, and the formation of a stable plug requires 2–3 plug-leakage cycles. The first and second cyclic plugging time was positively correlated with the fracture width. Different scales of fractures were successfully plugged with the bearing pressure greater than 6 MPa, but there were significant differences in the composition of the plugging layer. The experimental results can effectively prove that the utilized plugging agent is effective and provides an effective reference for dynamic plugging operation.

© 2025 The Authors. Publishing services by Elsevier B.V. on behalf of KeAi Communications Co. Ltd. This is an open access article under the CC BY-NC-ND license (http://creativecommons.org/licenses/by-nc-nd/4.0/).

#### 1. Introduction

The ongoing technological evolution within the hydrocarbon sector has precipitated a shift in exploration and production focus, transitioning from shallow formations to increasingly deeper stratigraphic reservoirs (Su et al., 2020; Zhang, 2020). Deep and ultra-deep well drilling operations encounter formidable geological constraints characterized by extreme thermobaric conditions, heightened in-situ stresses, and pervasive fracture networks, thereby inducing recurrent wellbore stability complications including but not limited to lost circulation, formation fluid influx, and borehole collapse. Drilling data reveals that lost circulation incidents constitute over 70% of non-productive time and operational complexity (Sun et al., 2021), resulting in not only substantial economic depletion but also compounded safety hazards

As a multicomponent hydrocarbon province, China's Ordos Basin exhibits complex structural architecture along its northern margin, encompassing three principal structural domains, specifically the Yishan Slope, Yimeng Uplift, and Tianhuan Depression, regions within which pervasive fluid migration pathways demonstrate significant spatial heterogeneity in leakage intensity (Jiang et al., 2024). Fracture-dominated leakage mechanisms prevail, with borehole image log interpretation revealing multiscale fracture systems spanning millimeter-to centimeter-scale apertures at depth. Advanced fluid loss control simulation systems, engineered per API 13B-1/ISO 10414 specifications, enable rational design of sealing slurry formulations through reconstructed fracture networks, thereby mitigating empirical uncertainty in field operations (Zhang, 2020). Contemporary apparatus configurations, such as bridging material testers (Nasiri et al., 2017), highpressure apparatus (Jeennakorn et al., 2017), and DL-series devices (Wang et al., 1997), share a consistent tripartite architecture composed of a pressure generation module, a fracture simulation chamber enabling aperture adjustment through interchangeable

E-mail address: zhangyq@cup.edu.cn (Y.-Q. Zhang).

Peer review under the responsibility of China University of Petroleum (Beijing).

and consequential production impairment (Xu et al., 2021; Bao, 2020).

<sup>\*</sup> Corresponding author.

spacer plates, and integrated real-time monitoring instrumentation. While permitting quantitative assessment of sealing efficacy across variable fracture widths, these systems exhibit persistent limitations including compromised experimental reproducibility, absence of dynamic pressure monitoring capabilities, and premature seal failure artifacts.

To elucidate fracture sealing mechanisms in fluid loss control. systematic experimental investigations have been conducted across multiple research paradigms. Yan et al. (2021) developed the DL-3A thermobaric evaluation system, which utilized dualphase bridging agents to simulate fracture conditions with circular apertures ranging from 1 to 5 mm and sealing slurry volumes of 2 L. In parallel, He et al. (2017) introduced a pressure-regulated visualization platform capable of dynamically adjusting fracture widths between 0 and 50 mm while maintaining control precision within  $\pm 2$  kPa, thereby enabling real-time observation of seal formation dynamics. Xu's research (Xu et al., 2023) achieved methodological breakthroughs through multiscale analysis, utilizing a microfluidic apparatus with 3–5 mm transparent fractures to quantify plugging kinetics at 0.6 mL/s flow rates. This approach defined sealing efficiency via temporal thresholds critical for stable barrier establishment. Complementing this, a tribological model incorporated shear failure mechanics within sealing matrices (Xu et al., 2019), identifying friction coefficients as critical determinants of plug integrity through finite element simulations of stress propagation.

Conventional fracture simulation templates are restricted by length limitations capped at 10 cm. a critical factor hindering comprehensive analysis of fluid containment dynamics. Researchers have further explored the microscopic bridging mechanism by improving the length of the plate or employing coupled CFD-DEM simulations. Yu (2014) pioneered macro-scale experimentation through a 30 cm full-diameter core module with 2 mm fractures under thermobaric conditions, enabling formulation optimization of sealing slurries. Building upon this, Calçada et al. (2015) engineered a 1.5 m fracture apparatus quantifying granular material performance while Wang et al. (2022) developed configurable 0.8×35 cm fracture systems with triaxial evaluation metrics. Transitioning to computational mechanics, Wu et al. (2025) established critical bridging thresholds through CFD-DEM analysis of flaky fibers in tortuous fractures, revealing force chain network integrity as the stability determinant. Concurrently, Lin et al. (2024) demonstrated thermal degradation mechanisms, which is that exposure in high temperature reduces particle friction coefficients and drilling fluid viscosity. Liu et al. (2023) optimized dynamic sealing through two key strategies: pressure differential window control and hybrid particle distributions with a D50 range spanning 50-150 µm, which significantly enhanced density in rough fracture environments. Ma et al. (2024) further advanced dual-porosity modeling, correlating permeability reduction in sealed zones with fracture reopening pressure enhancement.

Critical knowledge gaps persist in real-time sealing kinetics and micromechanical architectures of sealing matrices. Quantitative analysis of particulate migration dynamics and stress redistribution during barrier formation necessitates advanced fracture systems exceeding conventional length scales. Liu et al. (2023) developed a simulation device for leakage plugging of active-water and fissure-cavern, which consists of five parts: a fissure-cavern simulation system, a formation water simulation system, a plugging slurry injection system, a wellbore simulation system and a data acquisition system, etc. It can simulate a water flow rate of 10 m/min and a pressure resistance of 2 MPa. The leakage channel consists of a cement plate with a slit length of 30 mm, and the maximum plugging slurry dosage is 20 L.

Therefore, in response to the problems of smaller fracture length, non-dynamic cyclic plugging, metal fracture material and vertical fracture channel mentioned in the above research, the author conducted dynamic cyclic plugging experiments on large-scale fractures based on a self-developed dynamic plugging equipment. The experiments were conducted with cement cores more similar to the friction coefficient of the formation, and the fracture channels were oriented horizontally. The large-scale dynamic cyclic plugging experiments with different fracture widths and injection pressure parameters were conducted to analyze the influence of cyclic plugging time, pressure-bearing capacity and the formation of plugging layer. The experimental results can provide a basis for the design of cyclic plugging slurry and fracture cyclic plugging operation design.

## 2. Methodology

## 2.1. Mechanism of fracture plugging layer formation

The plugging of the leakage layer is realized by plugging slurry carrying material into fractures, and thus design of the slurry is the crucial for the process (Fig. 1). At present, there are many theories and rules about the design of bridging particle size of plugging materials, and different theories have their own scope of application. Commonly used theories and rules are 1/3 bridging theory, D50 rule, D90 rule, ideal filling theory and so on. In recent years, with the development of research techniques, a number of lost circulation material design methods for fracture have been proposed, as shown in Table 1. The new methods are based on fracture width, but each design method has significant differences. In this paper, the research is carried out according to the D90 rule for designing the grain size ration.

Meanwhile, in the complex downhole situation, the fracture width may change dynamically under the influence of wellbore pressure and other factors (Lee and Taleghani, 2020, 2022; Li et al., 2021; Wang et al., 2019), while the above material design methods are based on static fractures, making it difficult to match the variable fracture width (Feng et al., 2018; Zhu et al., 2019). Therefore, in this paper, we will also analyze the plugging effect in combination with the fracture mechanical aperture.

Aperture is the straight-line distance between the walls of a fracture and is a key parameter in determining the permeability and the design of the particle size of the plugging material. Laboratory-measured fracture apertures exhibit significant

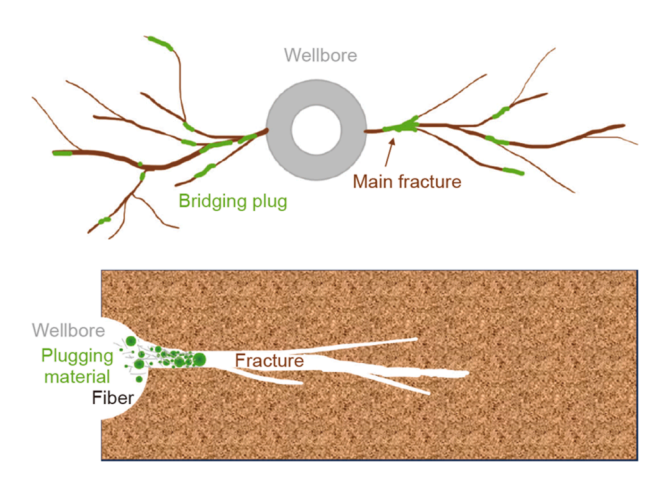


Fig. 1. Schematic diagram of bridging plugging mechanism for natural fractures.

**Table 1**Material design methods for fractures.

Number	Name	Results	Papers
1	D50 rule	D50 = fracture width	Whitfill, 2008
2	Updated D50 rule	D50 ≥ 3/10 fracture width	Alsaba et al., 2017
		D50 ≥ 6/5 fracture width	Razavi et al., 2016
3	Bimodal distribution	$CDF_{M,SD}(x) = \frac{1}{2} \left[ 1 + erf\left(\frac{\ln x - \mu}{\sigma\sqrt{2}}\right) \right]$	Razavi et al., 2010
4	D90 rule	The ratio of D90 of materials to fracture width should be 0.5–0.7	Wang et al., 2019
5	Porous medium	Fracture width $\leq 2000~\mu\text{m}$ , temperature $\leq 220~^{\circ}\text{F}$ , rotational speed $\leq 110~\text{rpm}$ ,	Ezeakacha and Salehi, 2018

enlargement compared to those under *in situ* conditions, a phenomenon attributed to stress release and resultant dilation during core retrieval (Wilhelmi and Somerton, 1967; Zeng, 2004). When the particle size of the plugging material is larger than the aperture, it tends to complete bridging and plugging outside fracture, forming a raised plugging area that prevents materials from entering the interior of the fracture. Therefore, an effective plugging layer is not formed inside the fracture, leading to plugging failure, which is called the entrance-plugging phenomenon (Fig. 2). It has the illusion of functioning temporarily. When the cycle is re-established, the plugging layer on the outside of the fracture is easily dislodged, leading to the reopening of the leakage channel and reoccurrence of leakage.

This paper derives the fracture mechanical aperture for downhole high-pressure conditions based on hydrodynamic theory. The analysis assumes (1) multi-fracture leakage is represented by an equivalent single fracture with established leakage-width relationships, (2) fracture length-to-width ratios exceed 10:1, and (3) drilling fluid behaves as an incompressible medium without wall seepage.

Assuming that the fracture is a parallel smooth infinite width narrow plate, a single width two-dimensional model is established as in Fig. 3. The continuity equation of incompressible fluid is established, and the newtonian fluid constitutive equation is introduced to establish the two-dimensional incompressible fluid N-S equation.

$$\frac{\partial(\rho v_1)}{\partial x} + \frac{\partial(\rho v_2)}{\partial y} = 0 \tag{1}$$

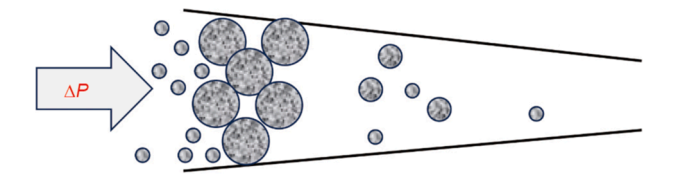


Fig. 2. Entrance-plugging phenomenon.

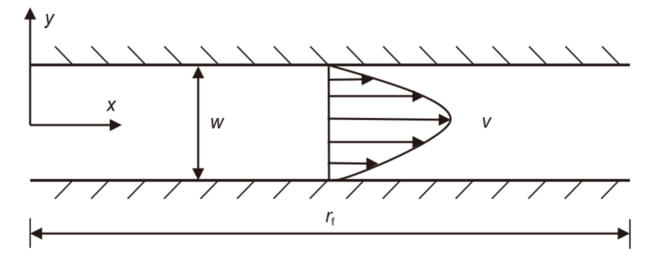


Fig. 3. A single width two-dimensional model.

$$\begin{cases}
v_1 \frac{\partial v_1}{\partial x} + v_2 \frac{\partial v_1}{\partial y} = f_X - \frac{1}{\rho} \frac{\partial P}{\partial x} + \mu \left( \frac{\partial^2 v_1}{\partial x^2} + \frac{\partial^2 v_1}{\partial y^2} \right) \\
v_1 \frac{\partial v_2}{\partial x} + v_2 \frac{\partial v_2}{\partial y} = f_X - \frac{1}{\rho} \frac{\partial P}{\partial y} + \mu \left( \frac{\partial^2 v_2}{\partial x^2} + \frac{\partial^2 v_2}{\partial y^2} \right)
\end{cases} (2)$$

The joint consideration of assumptions and boundary conditions, along with the application of the fractal method, is used to relate the fracture tortuosity (Zhang, 2020).

$$w_{\rm m} = w \delta^{\frac{1}{3}} = \sqrt{\frac{12\mu Q_{\rm f} r_{\rm f} \delta}{L\left[\left(\rho g - G_{\rm f}\right) H + \Delta P_{\rm a}\right]}}$$
(3)

where,  $w_{\rm m}$  is fracture mechanical aperture, m;  $\mu$  is fluid viscosity, Pa·s;  $Q_{\rm f}$  is the leakage volume of fracture section with width L, m³/s;  $r_{\rm f}$  is the length of mono-flanking fracture, m; L is the width of fracture, m;  $\delta$  is the tortuosity of the fracture;  $\rho$  is fluid density, kg/m³;  $G_{\rm f}$  is the stratigraphic pressure gradient, Pa/m; H is the depth of the leaking layer, m;  $\Delta P_{\rm a}$  is the wellbore annulus pressure depletion, Pa.

## 2.2. Experiment apparatus

Fracture aperture variations play a major role while drilling in fractured formations (Lavrov and Tronvoll, 2005). A decrease in wellbore pressure once circulation is stopped may lead to fracture closure. According to the similarity principle, a dynamic plugging simulation experimental apparatus (Fig. 4) for simulating the bridging-plugging process of fracture was developed in this study. The apparatus simulates the process of drilling fluid carrying plugging slurry into the fracture and evaluates the plugging effect of the slurry.

As shown in Fig. 5, the apparatus consists of a plugging testing vessel, a hydraulic power source, a working fluid synthesis system, a circulating pumping system, and a data acquisition and control system. The circulating pump system simulates the dynamic process of drilling fluid carrying lost circulation materials into fractures, supporting multiple plugging-leakage cycles to mimic downhole pressure fluctuations. The basic mechanism involves configuring, stirring, and heating the plugging material to a set temperature before transferring it into the hydraulic cylinder. Driven by a plunger pump, the slurry passes through a synthetic core, with a portion of the material retained within the fracture. The residual slurry is returned to the heated mixing system, continuing the cycle until the core is fully plugged and the system reaches the target working pressure. Based on experimental specifications, the apparatus integrates a large-scale synthetic core measuring up to 60 cm in length. This core is constructed with

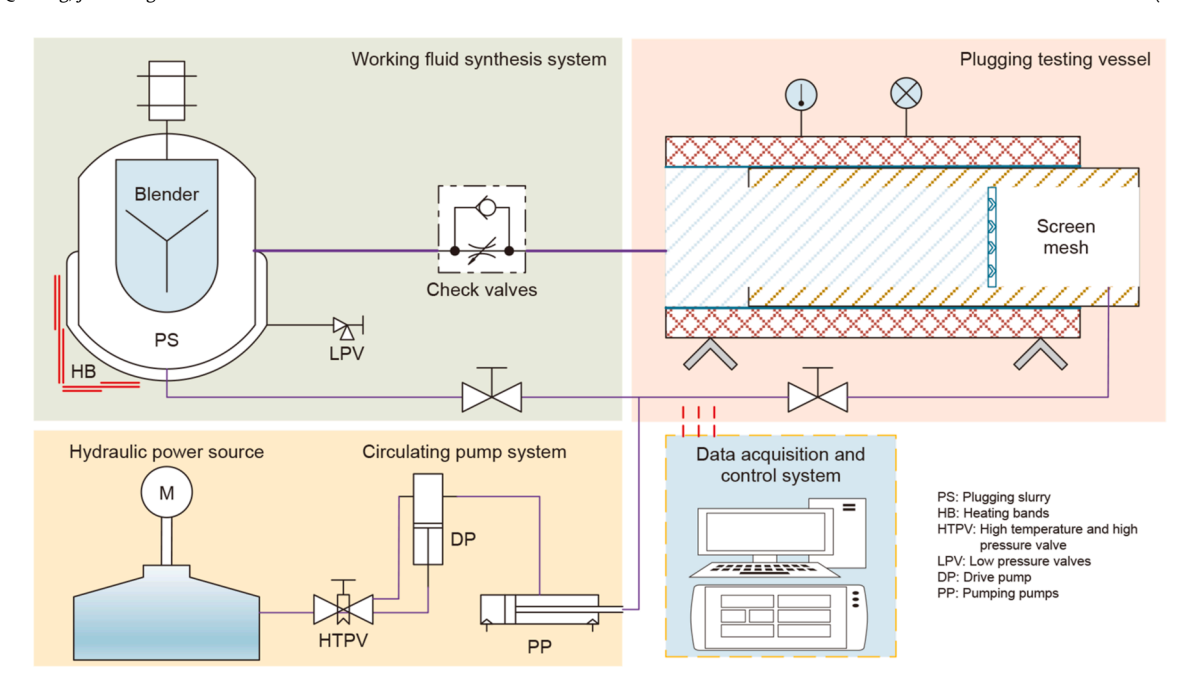


Fig. 4. Schematic of experimental equipment.

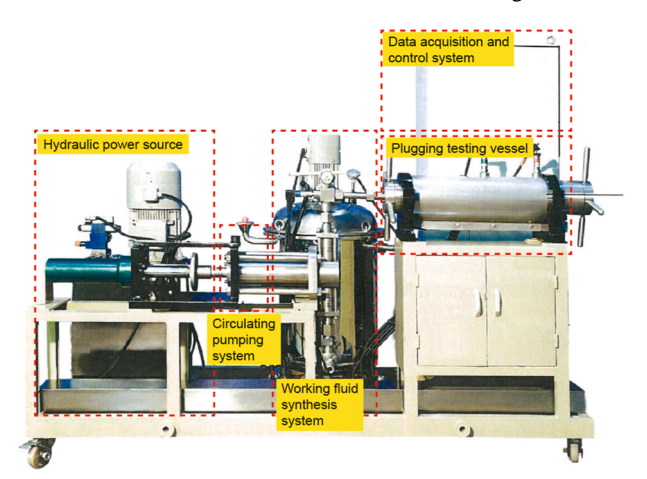


Fig. 5. Photo of dynamic plugging apparatus.

**Table 3** Synthetic core parameters.

Parameters		Unit	Value
Synthetic core	Diameter	cm	10
	Direction	/	Horizontal
Fracture	Width	mm	2–10
	Length	cm	50
	Туре	1	Curve

materials engineered to replicate key geological characteristics of actual lost circulation channels, including friction coefficient and porosity, thereby restoring stratum fracture physical parameters for dynamic plugging experimentation. The system operates within temperature and pressure ranges of 0–150  $^{\circ}\text{C}$  and 0–25 MPa, respectively. The injection rate of the apparatus is 6 L/min, the maximum stirring rate is 2900 r/min, and the volume of the working fluid synthesis system is 30 L.

**Table 2**Natural fracture width distribution and experimental rationale.

Width range, mm	Number	Proportion, %	Permeability, mD	Geological/engineering significance	Example cases
0.075–2.0	182	78	< 1	Low conductivity; limited impact on fluid flow	3725.3 m (0.075 mm)
2.0-10.0	45	19	1–100	Critical conductive fractures; dominant contributors to permeability	3960.0 m (10.76 mm)
					3856.1 m (3.76 mm)
> 10.0	6	3	> 100	Rare structural features; extreme scenarios	4210.0 m (21.68 mm)

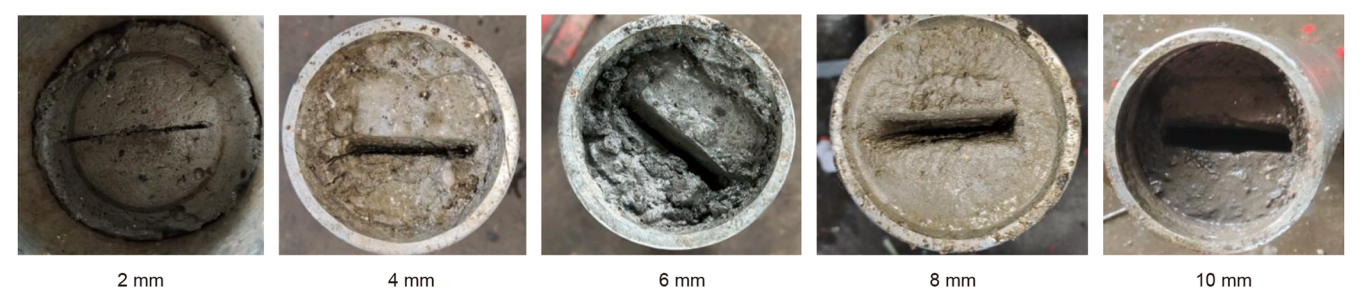


Fig. 6. Synthetic cores with different widths.

**Table 4** Hydrogel composition.

Marsh funnel viscosity, s	Density, g/cm <sup>3</sup>	$\theta_{600}$	$\theta_{300}$	Apparent viscosity, mPa·s	Plastic viscosity, mPa·s	Yield point, Pa	Particle suspension capacity
120	1.18	113.4	70.8	56.7	42.6	28.2	High (3–4 mm mica flakes, 5–6 mm nut shells)







Bentonite and CMC

Brown fiber

Micas

Fig. 7. Solid materials of plugging agent.

## 2.3. Experimental procedure

- a. Preparation of synthetic cores. Parameters such as particle size and strength of the core can be adjusted according to the characteristics of the zone and formation conditions, and the pattern including line and curve, and width of the fracture can also be regulated.
- b. Connect the relevant equipment for debugging and testing to ensure that systems in the experiment work properly.
- c. Based on the design of experiment, setting the injection parameters of the plugging slurry, including the initial pressure, displacement, and so on.
- d. Plugging slurry synthesis. The circulating slurry is prepared with on-site mud and solid materials, while CMC and powder are added to improve the viscosity. Before the experiment, the plugging system should be fully stirred until the powder is completely melted. During the process of the experiment, the leak plugging system could be adjusted in time according to the return of the slurry.
- e. Install the synthetic core into the plugging testing vessel and turn on the pump to circulate. Observe pressure gauges and sensor readings. The plugging process is a gradual bridging of materials, with the cyclic time increases the pressure increases gradually, after reaching the set parameters, the pump stops automatically. Observe each instrument to determine the plugging condition.
- f. During the experiment, if the values of the pressure sensors are all equal to 0, the bridge plugging process fails. The experiment can be stopped at this point.
- g. If the maximum pressure capacity needs to be tested, the set pressure value can be altered. It may also be removed and installed reversed with the synthetic core to test the reverse pressure capacity.
- h. The experimental device is dismantled, and photos are taken.

#### 2.4. Experimental materials

#### 2.4.1. Synthetic core

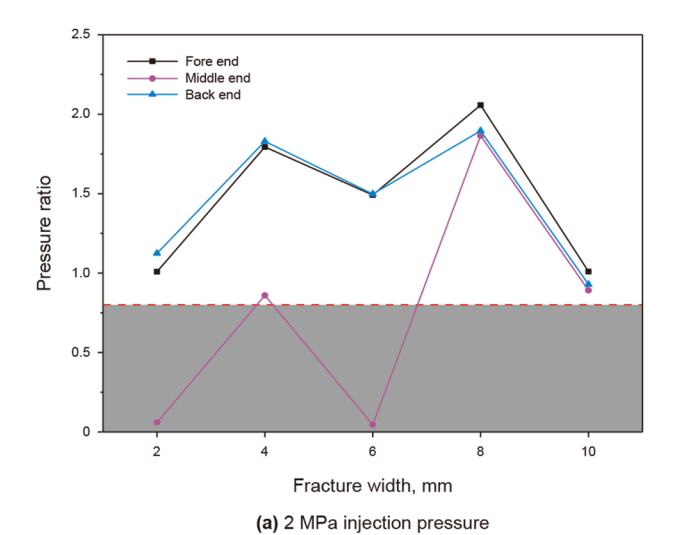
More severe fracture leakage exists in the northern margin of the Ordos Basin. The selection of the 2–10 mm fracture width range in our experiments was rigorously grounded in both geological characteristics of the Ordos Basin and hydraulic functionality of fractures. Field data from the studied wells reveal that natural fractures in the target formation exhibit aperture dimensions spanning from sub-millimeter scales, specifically 0.075 mm, to centimeter-scale features with examples reaching 21.68 mm at a depth of 4210.029 m (Table 2). Width distributions are predominantly clustered in the millimeter range between 0.075 and 10 mm. Notably, 78% of fractures fall within the 0.075-2.0 mm category. However, their ultranarrow apertures yield permeability values below 1 mD, contributing minimally to fluid flow. In contrast, fractures measuring 2-10 mm, accounting for 19% of the total population, demonstrate permeability magnitudes of 1-100 mD and dominate over 80% of the system's conductivity. A representative 10.76 mm fracture at 3960.017 m exemplifies this behavior with a permeability of 85 mD. Thus, the 2–10 mm range was prioritized to target fractures that are geologically representative, despite their lower abundance. Pressure fluctuations can make the fracture have a breathing effect, resulting in a larger fracture width. Experiments with millimeter-to centimeter-scale widths were designed based on the background. Experiments were conducted with five different fracture widths of 2, 4, 6, 8, and 10 mm (Fig. 6). Controlling the width as the only variable, the rest of the parameters, such as particle size, length, and gelatinizing time, were kept consistent. The fracture was uniformly set as Scurve. The core parameters are shown in Table 3.

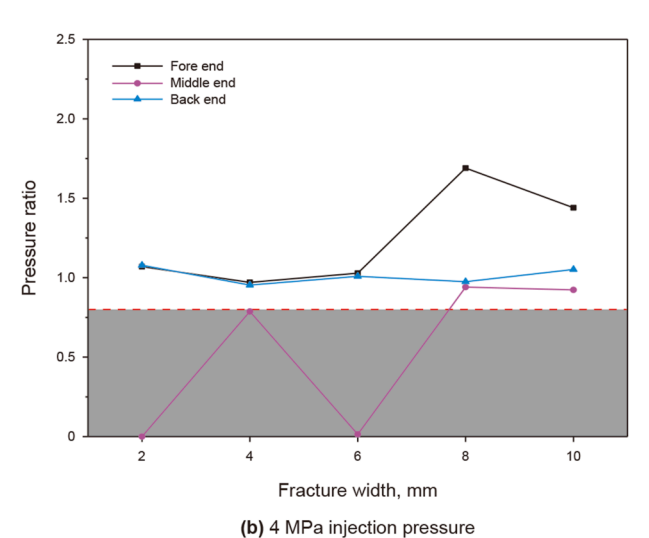
#### 2.4.2. Plugging material

The plugging slurry is the key to the dynamic cycling experiment and the suspension of the solid particles. After completing the slurry formulation, the rheological parameters of the plugging slurry were tested, as shown in Table 4.

**Table 5**Solid plugging agent composition.

Material type		Unit	Value
Slurry		kg	15
CMC		g	100
Water		g	600
Bentonite		g	173
Brown fiber	Length	mm	5–8
	Mass	g	32
Micas	Diameter 1	mm	0.5-0.65
	Diameter 2	mm	1.3–1.4
	Mass 1	g	170
	Mass 2	g	150





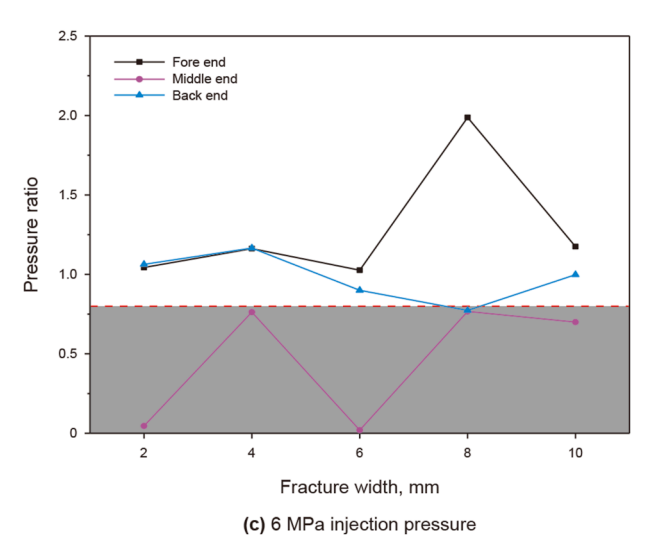


Fig. 8. Ratio of plugging pressure to injection pressure.

The experiments were conducted by using solid plugging material and pure gel material respectively. The solid material plugging agent contains slurry, high viscosity CMC, bentonite, water, brown fiber, vermiculite, and stirred for 15 min to make it well

**Table 6**Repeatable experiments.

Width, m	nm Conditions	Cyclic time	Plugging times	Pressure value
8	2 MPa/25 °C 2 MPa/25 °C		3	4.11/6.76/11.93 3.98/6.97/11.54
8	2 MPa/25 °C	, ,	3	4.24/6.55/12.32

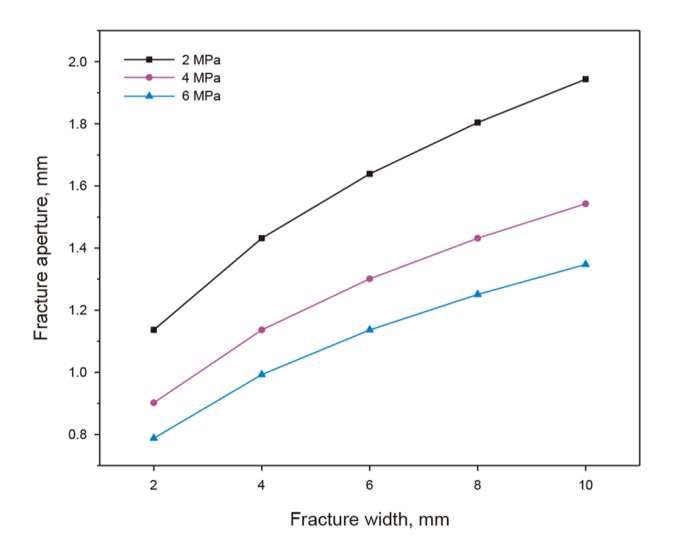


Fig. 9. Fracture mechanical aperture.

mixed (Fig. 7), and the dosage of the material is shown in the table below.

The selection of fiber and mica as plugging materials was guided by their intrinsic properties, geological compatibility, and operational demands. Fibers form a 3D network to fill fractures and adapt to dynamic aperture changes caused by the respiratory effect, while mica's flaky morphology provides rigid mechanical support under high pressure, synergistically enhancing bridging stability. This design aligns with the Ordos Basin's fracture characteristics, where millimeter-scale fractures dominate, but centimeter-scale ones locally develop. The composite system addresses field challenges, traditional granular materials often fail in high-conductivity fractures due to erosion, whereas the fiber-mica combination mitigates leakage via network flexibility and pressure-resistant filling, ensuring durability under cyclic pressure fluctuations. This rationale, supported by field data and material mechanics principles, has been incorporated into the experimental materials section.

Based on the results of Whitfill and Wang in Table 5, the D50 and D90 values of the solids were designed to be 0.65 and 1.4 mm for a width of 2 mm. The effectiveness of the formulation for larger widths of fractures under the dynamic plugging mechanism was investigated to analyze the adaptability.

According to the experimental results, the fracture plugging was analyzed by the ratio of plugging pressure and injection pressure, as shown in Fig. 8. The location of the plugging and the degree of densification varied under different conditions. Overall, each set of experiments resulted in the formation of dense plugs at the front and back ends, indicating that the formulation is well adapted to the dynamic plugging mechanism. The plugging in the middle end of the fracture shows significant differences. Three of the five particle sizes form a dense plugging layer with a coverage ratio exceeding 80% under a pressure of 2 MPa. With the gradual increase of pressure, the pressure ratio in the middle of the fracture is less than 80% at 6 MPa, forming a more loose plugging layer.

**Table 7** Entrance-plugging phenomenon statistics.

Width, mm	Length, m	Displacement, L/s	Tortuosity	Aperture, mm	Whether or not plugging at the entrance
2	0.5	0.1	1.6	1.136	Plugging, 2 times
				0.901	Plugging, 2 times
				0.788	Plugging, 2 times
4				1.432	Partially plugging, 2 times
				1.136	Partially plugging, 2 times
				0.993	Partially plugging, 2 times
6				1.639	Plugging, 2 times
				1.298	Plugging, 2 times
				1.136	Plugging, 2 times
8				1.804	Unplugged
				1.432	Unplugged
				1.251	Plugging
10				1.943	Unplugged
				1.542	Unplugged
				1.347	Partially plugging

**Table 8** Hydrogel composition.

Material type	Unit	Value
Main ingredients	g	950
Enhancer	g	300
Water	kg	5
Response agent	g	15

Although the material particle size design D50, D90 characteristic value only meets the 2 mm fracture width, but in the cyclic plugging process, the 4–10 mm wide fracture can also realize a well plugging effect. The way of circular plugging can effectively expand the range value of D50/D90 rule and relatively slow down the degree of entrance-plugging phenomenon.

## 2.5. Description of experimental reproducibility

To verify the reproducibility of the experiment, several replicated experiments were conducted for the 8 mm fracture width, and the plugging process and pressure-bearing performance of a fracture width were analyzed under the same conditions.

As show in Table 6, repeatability experiments showed a very high degree of similarity in the results, including the process of stabilizing the plugging layer formation as well as the plugging time. The pressure readings after the formation of the stabilized structure are also not very different. Their errors are all less than 5%.

## 3. Results and discussion

The process of forming a fracture plugging layer is generally regarded as multiple transport, retention and percolation filling of the plugging material, which eventually forms a stable layer to isolate the pressure in the fracture and the pressure of the wellbore liquid column, thus effectively controlling the leakage of wellbore working fluids (Yang et al., 2019). In this section, the results of experiments on plugging fractures with solid and gel materials are analyzed. A comparative analysis of the experiments of solid and gel materials for fracture plugging is also carried out.

### 3.1. Effect of fracture aperture on entrance-plugging

During the plugging process, the particle material is mixed in the plugging slurry, the wellbore pressure is higher than the formation pressure, and the slurry carries the material in a unidirectional flow state from the wellbore to the fracture. If the maximum diameter of the bridging particles in the plugging material is larger than the mechanical aperture of the fracture, entrance-plugging phenomenon may occur, thus blocking the entry of subsequent particles. The entrance-plugging phenomenon is analyzed by calculating the fracture mechanical aperture according to Eq. (3), and combining with the characteristic values of particle size D90 and D50.

From Fig. 9, at the same fracture width, the aperture decreases with increasing pressure. Under the same pressure condition, the aperture increases with the increase of width. Under the experimental conditions of this paper, the minimum value of fracture aperture is the value of width of 2 mm at pressure of 6 MPa, which is 0.788 mm, and the maximum value is the value of seam width of 10 mm at pressure of 2 MPa, which is 1.943 mm. Fracture aperture is affected by multiple factors such as pressure, width and length.

Entrance-plugging phenomenon is not only affected by the fracture aperture, but also has a great relationship with the design of the particle size of the plugging material. In this paper, D50 and D90 characteristic values of the solid particles of the plugging are counted and analyzed in combination with whether the entrance-plugging phenomenon occurs or not, and specific parameters are listed in the table below.

As shown in Table 7, varying degrees of entrance-plugging phenomena were observed during the experiment. Significant entrance-plugging occurs when the fracture aperture is  $\leq 1.3$ ,

**Table 9** Factors affecting gel formation.

Number	Time, h	Temperature, °C	Heating method	Gas tightness	Gelation status
1	6	120-140	Water bath	Hermetic	Gel achieved
2	5	120-140	Water bath	Hermetic	Gel achieved
3	4	120-140	Water bath	Hermetic	Gel achieved
4	3	120-140	Water bath	Hermetic	Gel achieved
5	3	100–120	Water bath	Hermetic	Gel achieved
6	2.5	100–120	Water bath	Gas-tight	Gel not achieved
7	2	100–120	Water bath	Non-gas-tight	Gel not achieved

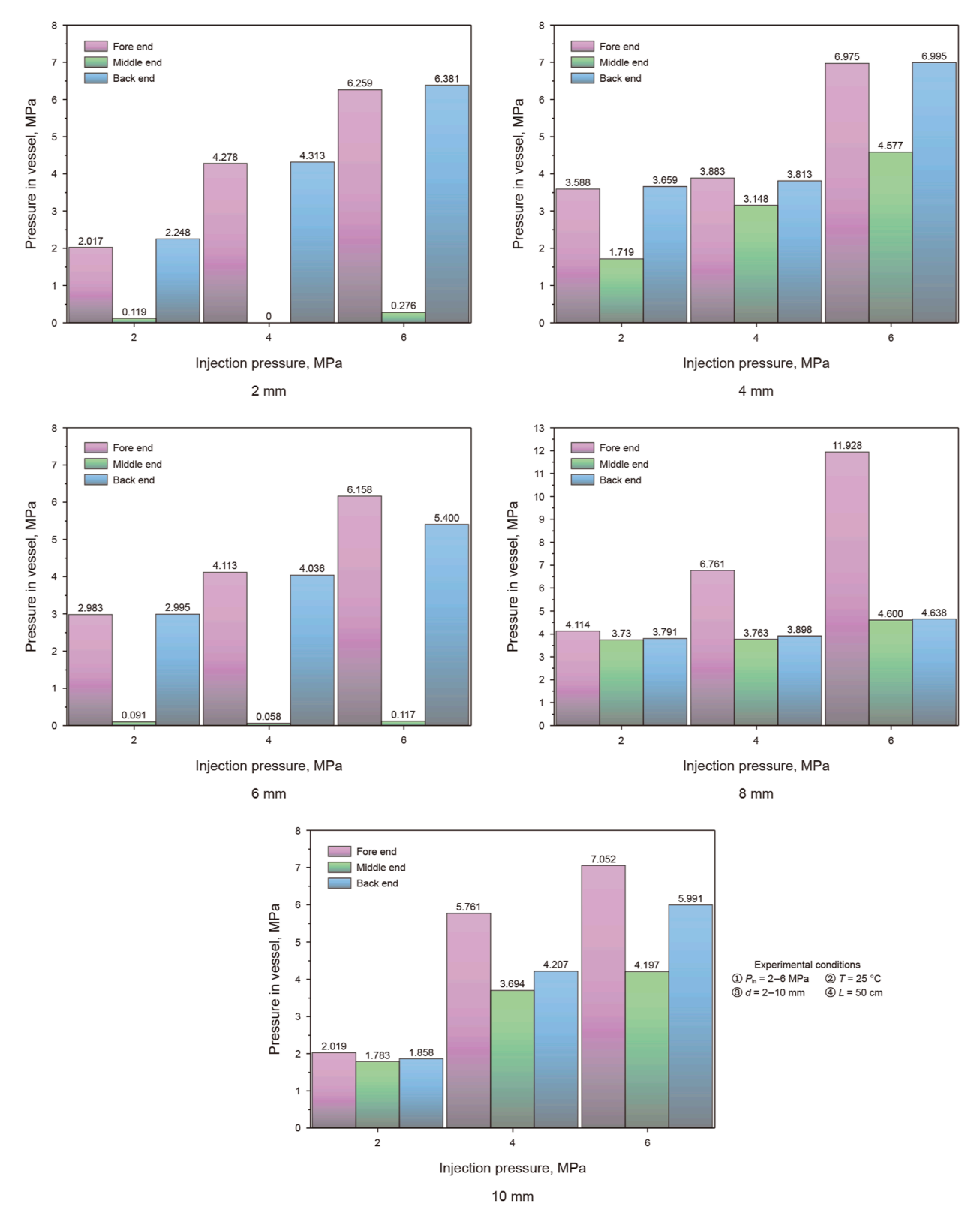


Fig. 10. Effect of differential pressure on plugging layer.

corresponding to twice the D50 particle size. Partial entrance-plugging develops when the aperture ranges from 1.3 to 1.4. Complete absence of entrance-plugging is observed when the aperture exceeds 1.4, equivalent to the D90 particle size.

When the width is 2 and 6 mm, both of them have a cavity in the middle, indicating that after the first formation of the plugging layer and then being pressed and leaked, the particles are transported to the vicinity of the outlet to form the plugging again. Subsequently, the particles at the front end piled up again to form the plugging layer. The particles could not stay in the center and could not enter the center. Therefore, it was judged that the entrance-plugging phenomenon occurred twice in the plugging process. The plugging process for a width of 4 mm was similar to that of 2/6 mm, but some of the material accumulated at its middle end to form a more transported plugging layer, but the entranceplugging phenomenon also occurred twice. The partially plugging phenomenon occurs when the fracture with a width of 10 mm has an entrance-plugging phenomenon of 1.348 mm under 6 MPa pressure, which is in the range of 1.3-1.4. This is manifested by the fact that its inlet and outlet pressures are almost equal to the injection pressure, while the pressure at the middle end is slightly smaller than the injection pressure, indicating an undense plugging layer in the middle. It is worth mentioning that the law summarized above is consistent with the overall law of 15 groups of experiments, and the prediction accuracy reaches 86.7%, among which two groups of experiments, on the other hand, have inconsistencies, respectively, the width of the fracture is 4 mm/ 2 MPa, and the width of the fracture is 6 mm/2 MPa. However, the entrance-plugging phenomenon from the fracture openings is still analyzed with a high accuracy.

#### 3.2. Effect of differential pressure on plugging results

Differential plugging pressure determines the pressure gradient between the inlet and outlet of the fracture, which affects the transportation behavior of the plugging material in the horizontal direction within the fracture, and has a significant effect on the plugging effect. In the research of previous scholars, the differential plugging pressure has a significant effect on the location of bridging, the length of plugging section and the porosity of plugging layer. Under the condition of 1 MPa, the length of plugging section is looser. Under the condition of 8 MPa, the length of the plugging layer is longer, and the shape of the plugging body is complete and dense (Bao, 2020). This section analyzes the effect of plugging layers of multiscale fractures at different plugging pressure differentials.

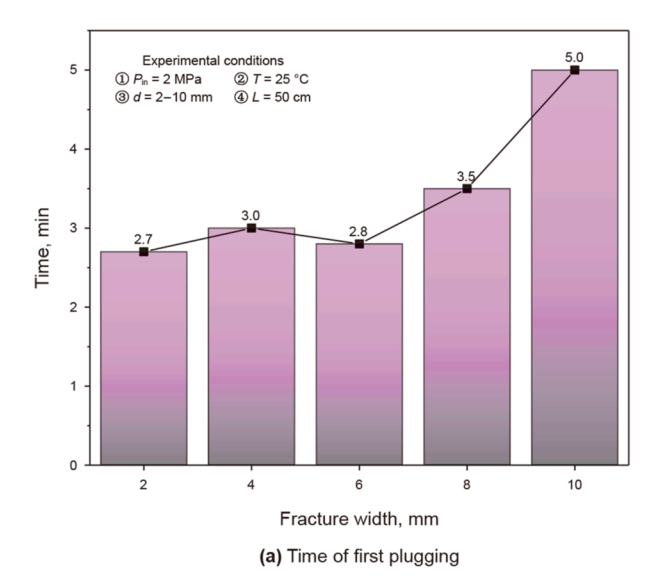
The effect on the fracture plugging process at different injection pressures is show in Fig. 10. Several injection pressures were set during the cyclic process, respectively 2, 4 and 6 MPa. The

experimental temperature was  $25\,^{\circ}\mathrm{C}$  and the length of the fracture was 50 cm. The pressure in the vessel is generally positively correlated with the injection pressure, indicating that plugging was achieved in all experiments for all slit widths, but with slight differences in their plugging characteristics. The experimental results for  $2–6\,\mathrm{mm}$  clearly show a trend of high pressure at the fore end and back end, and a low pressure in the middle. Whereas, 8 and 10 mm fracture widths show higher pressure at the fore end than at the middle and back ends. This indicates that the plugging layer of small size fracture is formed at the fore and back ends with a cavity in the middle, whereas the plugging layer of relatively large size fracture forms a plugging throughout the leakage channel.

For the 2 and 6 mm fracture, the formation of the middle cavity is due to the plugging at the fracture entrance phenomenon, which has been discussed in Section 3.1, so its plugging layer forms a relatively dense plugging layer at the fore and back ends. 4 mm fracture forms a relatively dense plugging layer throughout the leakage loss channel, the pressure at the fore and back ends is equal to the plugging pressure, and the central pressure value is smaller, but still can withstand a certain amount of pressure. And 8 and 10 mm fracture plugging effect is the best, in the whole leakage loss channel have formed a dense plugging layer, and the plugging pressure is basically the same. It is worth noting that the experimental results for the 4 mm fracture have a certain degree of chance. It indicates that the plugging at the fracture entrance phenomenon does not occur after reaching the conditions. This may be caused by the mechanism of dynamic plugging, because after plugging at the fracture entrance, there still exists the possibility of pressure leakage, thus restarting the whole plugging process.

## 3.3. Effect of different fracture widths on cyclic time

Solid bridging plugging agents generally consist of a mixture of several types of materials with a significant variation in their properties. Even for the same material of the same size, its shape is not regular and uniform. In the process of bridging plugging, there will be a certain degree of chance. This effect will affect the cyclic time of the experiment to some extent. Therefore, this paper conducted a regularity study on the cyclic time by using multiple repetitions of the experiment.



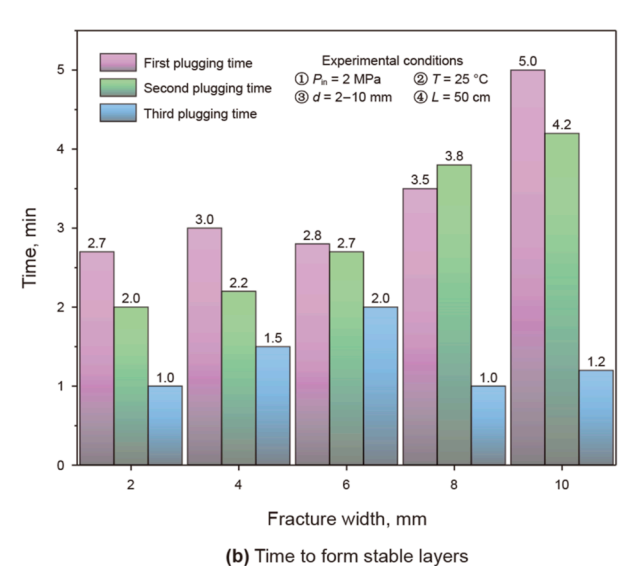


Fig. 11. Analysis of fracture plugging time with different scales.

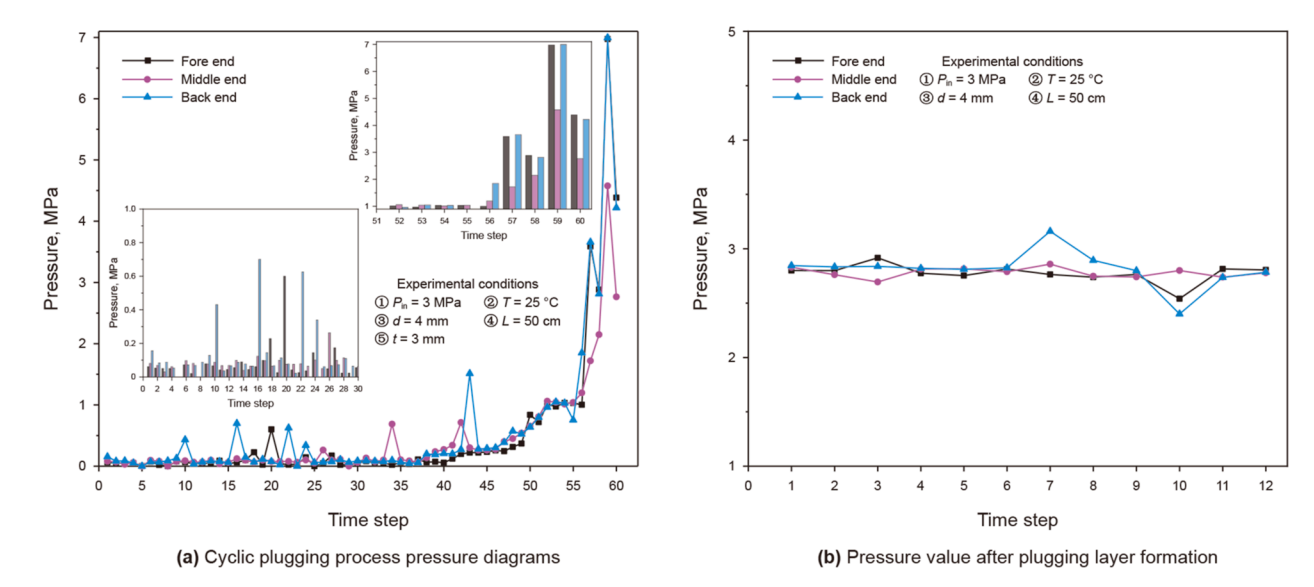


Fig. 12. Pressure fluctuation analysis.

Taking the cyclic time as the evaluation indicator, the synthetic core plugging law was explored for five curve fractures with the fracture widths of 2, 4, 6, 8, and 10 mm, respectively. The cycling process pumps the plugging system into the fracture at a constant rate, while the plugging material gradually bridges and fills all the fracture and pore spaces in the process, forming the plugging layer. Thus, it has strong inter-particle force to ensure that the established plugging layer has a strong ability to withstand wellbore pressure. The experimental results are shown in Fig. 11 below.

Fig. 11 shows the cyclic plugging process for synthetic cores with different fracture widths. As shown in Fig. 11(a), the cyclic time increased from 2.7 to 5 min as the fracture width increased from 2 to 10 mm, indicating that the cyclic plugging time increased with the increase of width. The irregular particles were transported, collided and flipped during the pumping process, and gradually stayed in the fracture in the form of bridging to form the

plugging layer. When the width of the fracture is less than or equal to 8 mm, the difference in cyclic plugging time varies slightly, indicating that the plugging formula can rapidly plugging the fractures below 8 mm, and its average cyclic time is 3 min. When the width increases to 10 mm, the cyclic time is up to 5 min, which is increased by 66.6%. In Fig. 11(b), the time required for the first and second plugging is positively correlated with the width, and the relationship between the third cycle time and the width is not obvious. After completing three plugging-leakage cycles, all synthetic cores were completely plugged, and the maximum bearing pressure could reach 10 MPa. The second cyclic plugging time increased gradually from a minimum of 2-4.2 min, while the third cyclic time was below 2 min. The results showed that the fracture was essentially completed filling of the fracture volume after two cycles, and a stable plugging layer could be formed after one more cycle. The process will go through several bridging-plugging-







Fig. 13. Schematic diagram of core taking out.



(a) Cores after the experiment



(b) 2 mm core section



4 mm-coir fiber
(c) 4 mm core section



(d) 6 mm core section



8 mm-coir fiber and vermiculite

(e) 8 mm core section

Fig. 14. Composition of the plugging layer.

leakage times during the cycles. Its pressure-bearing performance will be gradually improved because the material is constantly compacted in the process, thus improving the pressure-bearing capacity.

3.4. Effect of different fracture widths on pressure fluctuation

In this section, the pressure fluctuation of the cyclic plugging process is analyzed since bridging plugging is a gradual process.

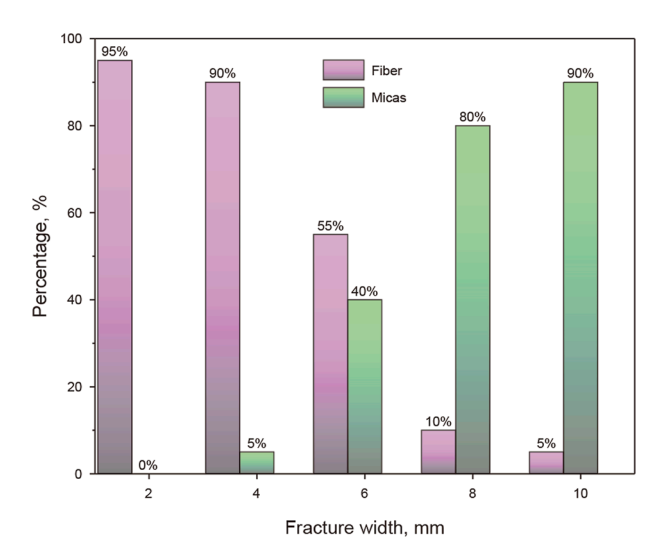


Fig. 15. Analysis of the composition of plugging layers.

The fracture plugging layer all showed pressure fluctuation during the horizontal loading process. That is, the pressure-bearing capacity varied due to small changes in the internal structure of the particles system and the movement of the plugging position. After the initial pressure changes, the pressurization was continued and the variation process was repeated (Kang et al., 2021; Ma et al., 2024).

Fig. 12 records the values of three sensors at the fore, middle and back end of the reactor during the cyclic plugging of the 4 mm fracture. The experimental conditions include an inlet pressure of 3 MPa, a temperature of 25 °C, a fracture length of 50 cm, a cyclic time of 3 min, and a total of 60 data points of pressure recorded. The pressure values in the vessel need to circle for a period before increasing. The graph shows that in time steps 1–50, the pressure values fluctuate within 0.3 MPa, and only a very few time steps are greater than 0.5 MPa. In time steps 50-55, the pressure values gradually increase to 0.8 MPa, and then rapidly increase to more than 4 MPa in the next 5 time steps. This phenomenon indicates that cyclic plugging is a process of material accumulation in the leakage channel, which can be divided into stage I material accumulation and stage II plugging formation. Stage I accounts for 90% of the time in the whole plugging process, while stage II plugging process only accounts for 10% of the time, and the pressure also increases rapidly in the last 10% of the time. At the same time, it should be noted that although the injection pressure is set to 3 MPa, the transient fluctuation value of reactor pressure reaches



Fig. 16. Unheated state of gel plugging agent.



Fig. 17. Gel state after heating in water.

6–7 MPa due to the compression effect of the material under high pressure and the uneven tightness of the leakage channel, which has a certain hysteresis. Fig. 12(b) shows the pressure values after the formation of the plugging layer, and it can be seen that the values fluctuate within the range of slightly less than the inlet pressure, which further supports the analysis that the plugging layer is gradually compacted during the bridging process.

Secondly, two sub-bar graphs for stage I and stage II are also shown in Fig. 12(a). They show the pressure variations at the front and middle ends of the vessel in time steps 1–30 and time steps 50–60, respectively. As can be seen from the plots, the pressures at the front and middle ends are almost less than 0.2 MPa during steps 1–20, indicating that the process material cannot accumulate at this point. In contrast, there are four moments at the back end that are greater than 0.5 MPa, where material accumulation starts from back to front. This can be demonstrated in the 56 time step, where the pressure values are significantly larger at the back end than at the front and middle ends, showing an increasing trend. In addition, there is a 56-60 time step pressure fluctuation phenomenon can be seen, the process of gradual pressurization after the formation of the plugging layer, the pressure value of the fore end and the back end is almost equal, while the pressure value of the middle is slightly smaller. This phenomenon indicates that the material formed a plugging layer at each of the fore end and back end, while the material in the middle was relatively untightened. That is, the build-up process starts initially at the back end of the vessel and gradually accumulates towards the middle and front ends. After a certain degree, the material could not enter smoothly, and then accumulated again at the fore end, thus causing the

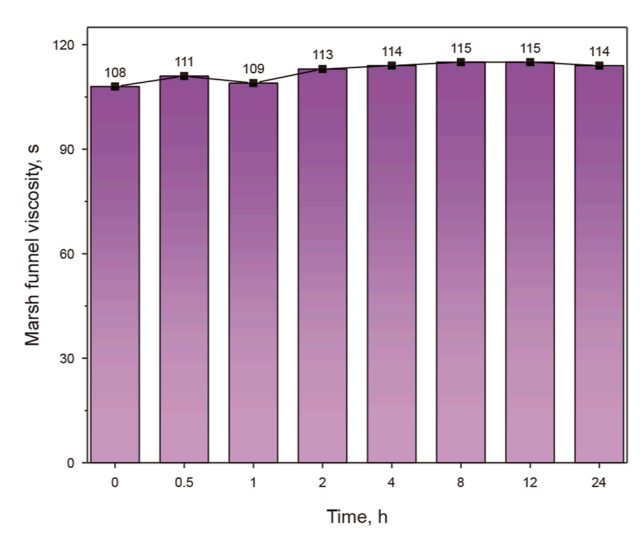


Fig. 18. Viscosity variation of gels.

**Table 10**Comparative analysis of different material.

Types of plugging agents	Heating in water	Pressurization	Width/length of fracture	Cyclic time min	Pressure-bearing capacity
Solid materials	1	Axis	10 mm/50 cm	5/4.2/0.2	> 6 MPa
Hydrogel-no cyclic	120 °C	Axis	10 mm/50 cm	1	0.3–0.4 MPa
	6 h				
Hydrogel-cyclic	120 °C	Axis	10 mm/50 cm	2.7/0.9/0	> 6 MPa
	6 h				

phenomenon that the pressure values were equal at both ends and small in the middle.

# 3.5. Effect of different fracture widths on composition of plugging layer

The insufficient strength of the plugging layer or the resulting false plugging also have a great impact on the efficient drilling operations. The main components of the plugging layer with different seam widths are obtained by analyzing the core sections after the completion of plugging operation.

After the completion of the experiment, the mold and the core were separated and the overall morphology of the core was observed, as shown in Fig. 13. It can be seen that the core still has a more complete morphology after the completion of the experiment, and the cross-section shows that there is a fracture filled with various plugging materials. After removing the core, the length of the core can be measured to be about 46 cm, which is 8% different from that before the experiment, and the preservation is complete.

Fig. 14(a)–(e) demonstrate the entire and sectional plugging morphology of the core. One can see the materials constituting the plugging layers of the cores are quite different. As shown in Fig. 14 (b) and (c), the main material filling in the 2 and 4 mm fracture is fiber, which occupies almost 90% of the composition. When the width increases to 6 mm, the mica begins to appear in the materials constituting the plugging layer and have a larger specific gravity of 40%. In the plugging layer with a width of 8 mm, more than 80% of the material is mica. Subsequently, the author measured the quality of the different materials, as shown in Fig. 15.

The formulations utilized in this experiment are highly adaptable and provide good plugging for a wide range of fracture scales. The discovery also provides a theoretical basis for the design of drilling fluid plugging slurry formulations.

## 3.6. Analysis of different plugging materials

The author also explored the effect of a hydrogel material on fracture plugging and compared it with rigid materials. The gel was first synthesized, and the process and components were as follows (see Tables 8 and 9).

Combine the ingredients and mix for 15 min as shown in Figs. 16 and 17. Subsequently, the prepared gel was poured into the synthetic core. The gel was heated by high temperature water bath, and condensed under high temperature 120 °C and pressure 2.5 MPa for 6 h, and the gel was jelly-like with certain viscoelasticity. After completing the heating, it was put into the reaction vessel and the gel was found to be airtight when installed.

By testing the viscosity of the gel, it can be found that its viscosity is relatively stable, and the difference between the viscosity after 24 h and that when the gel is just formed is very small, as show in Fig. 18. Secondly, the effects of gel coagulation time and temperature were investigated, and the results showed that the

gel can be formed into a gel with a minimum of 3 h coagulation in a water bath, and the temperature cannot be lower than 100  $^{\circ}$ C, at which time the gel has a good airtightness.

A comparative analysis of the pressure-bearing capacity of synthetic cores for 10 mm fracture in solid material plugging agent, hydrogel plugging agent without cyclic and hydrogel plugging agent with cyclic plugging is carried out in this section.

From Table 10, the composite plugging method is more effective for the plugging of large-scale fracture. When only solid materials are used, 3 cycles are required to form a stable plugging layer, and the total duration is about 10 min. When hydrogel is used without cycling, the material after forming the gel is soft, which has a certain degree of adhesion, but it cannot form a stable plugging layer, though it has a good airtightness. The pressure values at the fore and back ends showed some degree of difference, about 0.3–0.4 MPa. Using hydrogel combined with cyclic plugging, there is a significant increase in cyclic time, the cyclic time is reduced to 3.6 min, forming a stable plugging, the experimental process of pressure capacity greater than 6 MPa.

#### 4. Conclusion

Based on the large-scale curved fracture cyclic plugging experiments conducted under the conditions of this paper, the following conclusions are obtained.

- (1) The entrance-plugging phenomenon is predictable via fracture aperture analysis. Under dynamic cyclic plugging, entrance-plugging is avoidable when aperture exceeds the D90 threshold, whereas apertures smaller than 2 times the D50 value form central cavities.
- (2) Bridging by solid materials progresses gradually, requiring 2–3 plugging-leakage cycles for stable plugging layers. Plugging time correlates positively with fracture width.
- (3) Pressure fluctuations within the range of 0–0.3 MPa during cycling stabilize rapidly post-material accumulation, achieving a pressure-bearing capacities more than 6 MPa and an instantaneous maximum pressure of 11.9 MPa.
- (4) Plugging layer distribution varies with fracture width. 2–6 mm fractures exhibit dual-end plugging with midcavities, while 8–10 mm fractures form fore-end-dominant layers with mid-back low-pressure zones.
- (5) All tested fractures were successfully sealed using composite materials. Fiber-dominated layers adapt to narrow fractures (2–4 mm), transitioning to mica-dominated compositions (8–10 mm), demonstrating material adaptability for multi-scale fracture systems.

The current apparatus is specifically optimized to simulate dynamic plugging processes in isolated S-curved single fractures (lengths≤ 60 cm, widths 2–10 mm), yet its scalability to complex fracture networks, such as branching or intersecting systems, remains constrained by inherent design limitations. The synthetic

core fabrication process currently supports only predefined single-fracture geometries, while the fluid circulation system lacks independent control for multi-fracture flow partitioning or stress interaction modeling. Concurrently, there is still a lack of accurate and efficient analytical methods for the structure and components of the plugging layer after the experiments. The above deficiencies will be gradually improved in subsequent studies.

#### **CRediT authorship contribution statement**

**Zhao-Wen Hu:** Writing – review & editing, Writing – original draft, Investigation, Formal analysis, Data curation. **Yi-Qun Zhang:** Methodology, Funding acquisition, Conceptualization. **Jin-Shan Wang:** Data curation. **Xin-Yu Wang:** Writing – review & editing. **Yu Qin:** Validation. **Ya Liu:** Resources.

#### **Declaration of competing interest**

The authors declare that they have no known competing financial interests or personal relationships that could have appeared to influence the work reported in this paper.

#### Acknowledgments

This work was financially supported by National Natural Science Foundation of China (No. 52422402).

#### References

- Alsaba, M., Al Dushaishi, M.F., Nygaard, R., et al., 2017. Updated criterion to select particle size distribution of lost circulation materials for an effective fracture sealing. J. Petrol. Sci. Eng. 149, 641–648. https://doi.org/10.1016/j.petrol.2016.10.027.
- Bao, D., 2020. Study on tight sealing mechanism with high pressure bearing capacity and drilling fluid plugging technology in fractured formation. PhD thesis. China University of Petroleum-East China. https://doi.org/10.27644/d.cnki.gsydu.2020.000026 (in Chinese).
- Calçada, L.A., Neto, O.A., Magalhães, S.C., et al., 2015. Evaluation of suspension flow and particulate materials for control of fluid losses in drilling operation. J. Petrol. Sci. Eng. 131, 1–10. https://doi.org/10.1016/j.petrol.2015.04.007.
- Ezeakacha, C.P., Salehi, S., 2018. Experimental and statistical investigation of drilling fluids loss in porous media–part 1. J. Nat. Gas Sci. Eng. 51, 104–115. https://doi.org/10.1016/j.jngse.2017.12.024.
- Feng, Y., Li, G., Meng, Y., 2018. A coupled CFD-DEM numerical study of lost circulation material transport actual rock fracture flow space. In:IADC/SPE Asia Pacific Drilling Technology Conference and Exhibition, Bangkok, Thailand. https://doi.org/10.2118/191098-MS.
- Jeennakorn, M., Nygaard, R., Nes, O.M., et al., 2017. Testing conditions make a difference when testing LCM. J. Nat. Gas Sci. Eng. 46, 375–386. https://doi.org/ 10.1016/j.jngse.2017.08.003.
- He, Y.C., Han, T.F., Zhao, J.G., et al., 2017. Development of high temperature and high pressure visible leakage plugging instrument. Equip. Geotech. Eng. 18 (1), 24–26. https://doi.org/10.3969/j.issn.1009-282X.2017.01.006 (in Chinese).
- Jiang, X.L., Li, M.Z., Zhang, J.Y., 2024. Key technologies for drilling and completion engineering of Dongsheng Gas Field in Ordos. Moder. Chem. Res. 18 (7), 102–104. https://doi.org/10.20087/i.cnki.1672-8114.2024.07.032 (in Chinese).
- 102–104. https://doi.org/10.20087/j.cnki.1672-8114.2024.07.032 (in Chinese). Kang, Y.L., Jing, H.R., Xu, C.Y., et al., 2021. Effects of particle shape on the mesostructure stability of fracture plugging zones. J. Southwest Petrol. Univ (Sci. Technol. Edit.) 43 (3), 81–92. https://doi.org/10.11885/j.issn.1674-5086.2020.12.20.02 (in Chinese).
- Lavrov, A., Tronvoll, J., 2005. Mechanics of borehole ballooning in naturally-fractured formations. SPE Middle East Oil and Gas Show and Conference, Manama, Bahrain. https://doi.org/10.2118/93747-MS.
- Lee, L., Taleghani, A.D., 2020. Simulating fracture sealing by granular LCM particles in geothermal drilling. Energies 13 (18), 4878. https://doi.org/10.3390/en13184878.
- Lee, L., Taleghani, A.D., 2022. Assessment of lost circulation material particle-size distribution on fracture sealing: a numerical study. SPE Drill. Complet. 37 (3), 191–205. https://doi.org/10.2118/209201-PA.
- Li, J., Qiu, Z.S., Zhong, H.Y., et al., 2021. Optimizing selection method of continuous particle size distribution for lost circulation by dynamic fracture width evaluation device. J. Petrol. Sci. Eng. 200, 108304. https://doi.org/10.1016/j. petrol.2020.108304.
- Lin, C., Xu, Q.C., Han, L.X., et al., 2024. Fracture sealing performance of granular lost circulation materials at elevated temperature: a theoretical and coupled CFD-

- DEM simulation study. Pet. Sci. 21 (1), 567–581. https://doi.org/10.1016/j.petsci.2023.10.002.
- Liu, Y.Q., Dong, M.L., Cai, K.C., et al., 2023a. Study on particle plugging in propagating fractures based on CFD-DEM. Front. Earth Sci. 10, 1037532. https://doi.org/10.3389/feart.2022.1037532.
- Liu, J.H., Li, D.Q., Li, F., et al., 2023b. Simulation device and experimental study on leakage and plugging of active water fracture hole. Drill. Fluid Complet. Fluid 40 (2), 169–175. https://doi.org/10.12358/j.issn.1001-5620.2023.02.004 (in Chinese).
- Ma, C.Y., Feng, Y.C., Dou, Y.H., et al., 2024a. Experimental study on the design method of lost circulation materials for induced fractures. Geoenergy Sci. Eng. 240, 213086. https://doi.org/10.1016/j.geoen.2024.213086.
- Ma, Y.L., Wan, L., Hou, W., et al., 2024b. Geomechanical analysis of lost circulation control in tight formations. Front. Earth Sci. 12, 1349634. https://doi.org/ 10.3389/feart.2024.1349634.
- Nasiri, A., Chaffarkhah, A., Moraveji, M.K., et al., 2017. Experimental and field test analysis of different loss control material for combating lost circulation in bentonite. J. Nat. Gas Sci. Eng. 44 (4), 1–8. https://doi.org/10.1016/j. ingse.2017.04.004.
- Razavi, O., Vajargah, A.K., Van Oort, E., et al., 2016. Optimum particle size distribution design for lost circulation control and wellbore strengthening. J. Nat. Gas Sci. Eng. 35, 836–850. https://doi.org/10.1016/j.jngse.2016.08. 038
- Su, Y.N., Lu, B.P., Liu, Y.S., et al., 2020. Status and research suggestions on the drilling and completion technologies for onshore deep and ultra-deep wells in China. Oil Drill. Product. Technol. 42 (5), 527–542. https://doi.org/10.13639/j.odpt.2020.05.001 (in Chinese).
- Sun, J.S., Bai, Y.R., Cheng, R.C., et al., 2021. Research progress and prospect of plugging technologies for fractured formation with severe lost circulation. Petrol. Explor. Dev. 48 (3), 630–638. https://doi.org/10.1016/S1876-3804(21) 60059-9 (in Chinese).
- Wang, D.Y., Shi, T.H., Lu, X.T., 1997. Development and design of DL-1 leakage plugging experimental device. J. Southwest Pet. Inst. 19 (2), 51–54. https://doi.org/10.3863/j.issn.1000-2634.1997.02.11 (in Chinese).
- Wang, G., Huang, Y.J., Xu, S.J., 2019. Laboratory investigation of the selection criteria for the particle size distribution of granular lost circulation materials in naturally fractured reservoirs. J. Nat. Gas Sci. Eng. 71, 103000. https://doi.org/10.1016/j.jngse.2019.103000.
- Wang, Z.X., Ou, T., Han, Q., et al., 2022. The conception and design of multi-mode core drilling leak plugging test device. Acta Geol. Sichuan 42 (S1), 74–78. https://doi.org/10.3969/j.issn.1006-0995.2022.S1.015 (in Chinese).
- Whitfill, D., 2008. Lost circulation material selection, particle size distribution and fracture modeling with fracture simulation software. In:Asia Pacific Drilling Technology Conference and Exhibition, Jakarta, Indonesia. https://doi.org/10. 2118/115039-MS.
- Wilhelmi, B., Somerton, W.H., 1967. Simultaneous measurement of pore and elastic properties of rocks under triaxial stress conditions. Soc. Petrol. Eng. J. 7 (3), 283–294. https://doi.org/10.2118/1706-PA.
- Wu, L.S., Liu, Y.X., Guo, J.C., et al., 2025. CFD-DEM simulation of composite plugging using novel sheet fibers in rough fractures. Energy 319, 134895. https://doi.org/ 10.1016/j.energy.2025.134895.
- Xu, C.Y., Zhang, J.Y., Kang, Y.L., et al., 2021. Structural formation and evolution mechanisms of fracture plugging zone. Petrol. Explor. Dev. 48 (1), 202–210. https://doi.org/10.1016/S1876-3804(21)60019-8 (in Chinese).
- Xu, C.Y., Zhang, H.L., She, J.P., et al., 2023. Experimental study on fracture plugging effect of irregular-shaped lost circulation materials. Energy 276, 127544. https://doi.org/10.1016/j.energy.2023.127544.
- Xu, C.Y., Yan, X.P., Kang, Y.L., et al., 2019. Friction coefficient: a significant parameter for lost circulation control and material selection in naturally fractured reservoir. Energy 174, 1012–1025. https://doi.org/10.1016/j. energy.2019.03.017.
- Yan, J.F., Wu, J.S., Jiang, B., et al., 2021. Development of a device for evaluating lost circulation materials at high temperature high pressure. Drill. Fluid Complet. Fluid 38 (2), 212–217. https://doi.org/10.3969/j.issn.1001-5620.2021.02.014 (in Chinese).
- Yang, C., Zhou, F.J., Feng, W., et al., 2019a. Plugging mechanism of fibers and particulates in hydraulic fracture. J. Petrol. Sci. Eng. 176, 396–402. https://doi.org/10.1016/j.petrol.2019.01.084.
- Yang, X.Y., Chen, S.Y., Shi, Y.P., et al., 2019b. CFD and DEM modelling of particles plugging in shale pores. Energy 174, 1026–1038. https://doi.org/10.1016/j. energy.2019.03.050.
- Yu, H.F., 2014. Experimental Simulation of Sealing Leakage in Fractured Reservoirs and Optimization of Sealing Grout Formula. Master's Thesis. Southwest Petroleum University (in Chinese).
- Zeng, L., 2004. Fractures and their seepage characteristics in low-permeability sandstone oil and gas reservoirs. Chin. J. Geol. 39 (1), 11–17. https://doi.org/10.3321/j.issn:0563-5020.2004.01.002 (in Chinese).
- Zhang, J., 2020a. Study on the mechanism and key technology of fracture leakage plugging while drilling in Coal Mining Area. PhD Thesis. China Coal Research Institute. https://doi.org/10.27222/d.cnki.gmkzy.2020.000007 (in Chinese).
- Zhang, S., 2020b. Study on Lost Circulation Mechanism and Control Formulation in multi-scale Fracture Formation. PhD Thesis. China University of Petroleum-Beijing. https://doi.org/10.27643/d.cnki.gsybu.2023.001390 (in Chinese).
- Zhu, B.Y., Tang, H.M., Wang, X., et al., 2019. Coupled CFD-DEM simulation of granular LCM bridging in a fracture. Part. Sci. Technol. 38 (3), 371–380. https:// doi.org/10.1080/02726351.2018.1547341.